The FASEB Journal
The Journal of the Federation of American Societies for Experimental Biology
All Articles | Submit | Subscribe | What's New | RSS

FASEB J. 2018 Feb; 32(2): 782–794.
Published online 2017 Oct 13. doi: 10.1096/fj.201700220RR: 10.1096/fj.201700220RR
PMCID: PMC5888396
PMID: 29030399

Robust lysosomal calcium signaling through channel TRPML1 is impaired by lysosomal lipid accumulation

Néstor Más Gómez,[*] Wennan Lu,[*] Jason C. Lim,[*] Kirill Kiselyov,[†] Keith E. Campagno,[*] Yulia Grishchuk,[‡§] Susan A. Slaugenhaupt,[‡§] Bruce A. Pfeffer,[¶‖#**] Steven J. Fliesler,[¶‖#**] and Claire H. Mitchell[*††‡‡,1]

[*]Department of Anatomy and Cell Biology, University of Pennsylvania, Philadelphia, Pennsylvania, USA;
[†]Department of Biological Science, University of Pittsburgh, Pittsburgh, Pennsylvania, USA;
[‡]Center for Genomic Medicine, Massachusetts General Hospital Research Institute and Harvard Medical School, Boston, Massachusetts, USA;
[§]Department of Neurology, Massachusetts General Hospital Research Institute, Harvard Medical School, Boston, Massachusetts, USA;
[¶]Department of Ophthalmology, Ross Eye Institute, Jacobs School of Medicine and Biomedical Sciences, State University of New York (SUNY)–University at Buffalo, Buffalo, New York, USA;
[‖]Department of Biochemistry, Jacobs School of Medicine and Biomedical Sciences, State University of New York (SUNY)–University at Buffalo, Buffalo, New York, USA;
[#]State University of New York (SUNY)–Eye Institute, Buffalo, New York, USA;
[**]Research Service, Veterans Affairs Western New York Healthcare System, Buffalo, New York, USA;
[††]Department of Ophthalmology, University of Pennsylvania, Philadelphia, Pennsylvania, USA;
[‡‡]Department of Physiology, University of Pennsylvania, Philadelphia, Pennsylvania, USA
[1]Correspondence: Department of Anatomy and Cell Biology, University of Pennsylvania, 440 Levy Building, 240 S. 40th St., Philadelphia, PA 19104-6030, USA., E-mail: chm@upenn.edu

Received 2017 Mar 22; Accepted 2017 Sep 26.

Abstract

The transient receptor potential cation channel mucolipin 1 (TRPML1) channel is a conduit for lysosomal calcium efflux, and channel activity may be affected by lysosomal contents. The lysosomes of retinal pigmented epithelial (RPE) cells are particularly susceptible to build-up of lysosomal waste products because they must degrade the outer segments phagocytosed daily from adjacent photoreceptors; incomplete degradation leads to accumulation of lipid waste in lysosomes. This study asks whether stimulation of TRPML1 can release lysosomal calcium in RPE cells and whether such release is affected by lysosomal accumulations. The TRPML agonist ML-SA1 raised cytoplasmic calcium levels in mouse RPE cells, hesRPE cells, and ARPE-19 cells; this increase was rapid, robust, reversible, and reproducible. The increase was not altered by extracellular calcium

removal or by thapsigargin but was eliminated by lysosomal rupture with glycyl-L-phenylalanine-β-naphthylamide. Treatment with desipramine to inhibit acid sphingomyelinase or YM201636 to inhibit PIKfyve also reduced the cytoplasmic calcium increase triggered by ML-SA1, whereas RPE cells from TRPML1$^{-/-}$ mice showed no response to ML-SA1. Cotreatment with chloroquine and U18666A induced formation of neutral, autofluorescent lipid in RPE lysosomes and decreased lysosomal Ca^{2+} release. Lysosomal Ca^{2+} release was also impaired in RPE cells from the ATP-binding cassette, subfamily A, member 4$^{-/-}$ mouse model of Stargardt's retinal dystrophy. Neither TRPML1 mRNA nor total lysosomal calcium levels were altered in these models, suggesting a more direct effect on the channel. In summary, stimulation of TRPML1 elevates cytoplasmic calcium levels in RPE cells, but this response is reduced by lysosomal accumulation.—Gómez, N. M., Lu, W. Lim, J. C., Kiselyov, K., Campagno, K. E., Grishchuk, Y., Slaugenhaupt, S. A., Pfeffer, B., Fliesler, S. J., Mitchell, C. H. Robust lysosomal calcium signaling through channel TRPML1 is impaired by lysosomal lipid accumulation.

Keywords: cellular aging, calcium signaling, lysosomal storage disease, RPE, mucolipin

---

Lysosomes are acidic intracellular organelles traditionally known for their degradation of macromolecules. More recently, lysosomes have been recognized as the second largest store of intracellular Ca^{2+} in cells (1, 2–3). The release of lysosomal calcium has been implicated in numerous functions central to cellular well-being, including lysosomal exocytosis (4), lyso-endosomal fusion (5, 6), the activation of transcription factor EB (TFEB) (7, 8), and the regulation of oxidative stress (9). The transient receptor potential mucolipin 1 (TRPML1) cation channel resides on late-endosomal/lysosomal membranes and provides a pore for lysosomal calcium efflux (1, 2, 10). Mutations in *MCOLN1*, the gene that encodes TRPML1, are responsible for causing mucolipidosis type IV (MLIV), a severe lysosomal storage disorder (11). This degenerative disease presents with delayed psychomotor development and neural pathologies including retinal degeneration, with vision loss common in the second decade (12, 13–14). Retinal dysfunction with thinning of the photoreceptor cell layer was recently described in the TRPML1$^{-/-}$ mouse model for MLIV (15).

Although the photoreceptors have a direct contribution to vision, their support by retinal pigment epithelial (RPE) cells is also necessary for optimal sight. RPE cells must process the phagocytosed tips of photoreceptor outer segments that are shed daily, in addition to their own autophagic material (16). This gives them one of the highest degradative loads in the body and makes the defects in the efficiency of lysosomal degradation readily apparent. Incomplete degradation of cellular waste by RPE lysosomes leads to the accumulation of oxidized lipids, accompanied by the formation of lipofuscin granules. Lysosomal stress, as manifest by agents that elevate lysosomal pH or interfere with transport, has been shown to increase lipofuscin accumulation in *in vitro* and *in vivo* models of retinal degeneration, including the ATP-binding cassette, subfamily A, member 4 (ABCA4)$^{-/-}$ mouse model of recessive Stargardt's disease (17, 18–19) and chloroquine (CHQ) retinopathy (20).

Given the central role of RPE lysosomes and autophagy in photoreceptor health (21, 22) and the contribution of TRPML1 to lysosomal regulation (8, 23), we examined the effect of TRPML1 activation in RPE cells and asked whether this was impaired by lipid accumulation in the lysosome. The

study confirms a key role for TRPML1 in lysosomal calcium signaling in RPE cells and suggests this release is impaired by accumulation of lysosomal material.

MATERIALS AND METHODS

Mouse RPE cells

All mice were treated in accordance with University of Pennsylvania IACUC in compliance with the Public Health Service Policy on Humane Care and Use of Laboratory Animals. Mice were reared at 5–15 lux and euthanized with a CO_2 overdose. Eyes from mice of both sexes were isolated and processed as described in Guha *et al*. (24). In brief, after enucleation, retinas were removed, and the eyecup was rinsed with Versene (Dow Chemical, Midland, MI, USA) and incubated in 0.25% trypsin for 1 h. Isolated mRPE cells were grown in DMEM/F12 Media (11330; Thermo Fisher Scientific, Waltham, MA, USA) containing 10% fetal bovine serum (FBS) (Thermo Fisher Scientific) and 1% 100 g/ml penicillin/streptomycin (15140-122; Thermo Fisher Scientific). C57Bl/6J mice were obtained from The Jackson Laboratory (Bar Harbor, ME, USA). TRPML1$^{-/-}$ mice were obtained from Susan Slaugerhaupt (Harvard University, Cambridge, MA, USA). Mice were genotyped for TRPML1 using the following primers as described in Venugopal *et al*. (13): WT forward, GACCCAGGAATGACACCTTC; WT reverse, CCCCTTGCTGCCATGTAATA; TRPML1$^{-/-}$ reverse, GCGCAAACCACATGTGCTTT. The knockout was detected using the following primers against the missing exon 3: forward, CTCATTCTCTTTGGGCTCAG; reverse, TATTCCCTCAACCCCCTAAC; product length 203 bp. ABCA4$^{-/-}$ mice were obtained from Gabriel Travis (University of California, Los Angeles, Los Angeles, CA, USA) and were genotyped using the following primers: forward, TGCCCGCACTTGTGTATTTA; reverse, AGAAGGGTGTCATCCTGTGG and for RPE65 using primers forward, ATGACTGAGAAGAGGATTGTC; reverse, CTGCTTTCAGTGGAGGGATC (25) (Supplemental Fig. 1). All mice were negative for the RD8 mutation (26).

Human embryonic stem cell–derived RPE cells cells

Human embryonic stem cell–derived RPE cells (hesRPE) [strain En74, derived from the H9 hesc line; National Institutes of Health (NIH; Bethesda, MD, USA) registration number 0062] were provided by Lincoln Johnson (Laboratory for Stem Cell Biology and Engineering, Neuroscience Research Institute, University of California, Santa Barbara, Santa Barbara, CA, USA) and generated as described in Rowland *et al*. (27). Briefly, the differentiation of the stem cells to RPE was carried out using defined medium (X-Vivo 10; Lonza, Walkersville, MD, USA) while being maintained on a substrate of Matrigel (BD Biosciences, Franklin Lakes, NJ, USA) as the only animal-derived system component. Pigmented foci were isolated by dissection and dissociated using TrypLE Express (Thermo Fisher Scientific). First-passage subcultures were established on Synthemax substrate (Corning, Corning, NY, USA) before further dissociation and cryopreservation for shipment. Second-passage hesRPE cells were thawed and plated on poly-L-ornithine (Sigma-Aldrich, Saint Louis, MO, USA)–coated tissue culture plastic, and these cultures were expanded for up to 3 additional passages using previously described methods (28). Briefly, proliferation in partially defined [1% (v/v) bovine calf serum, Lonza; 0.5% saline extract of bovine retina crude homogenate con-

tributing added protein in final medium = 6 mg/L] growth medium containing total Ca^{2+} of <0.1 mM gave rise to detached, suspended cells that were harvested nonenzymatically for either further subculture or cryopreservation.

ARPE-19 cells

ARPE-19 cells (American Tissue Type Collection, Manassas, VA, USA) were grown as previously described (29). In brief, cells were grown in 1:1 mixture of DMEM and Ham's F12 medium with 3 mM L-glutamine, 100 g/ml streptomycin, and 10% FBS (all from Thermo Fisher Scientific). Cells were incubated at 37°C in 5% CO_2 and subcultured weekly with 0.05% trypsin and 0.02% EDTA.

Human MLIV fibroblasts

Healthy human fibroblasts (GM03440) and MLIV fibroblasts (GM02048) from a patient with MLIV were obtained from the Coriell Institute (Camden, NJ, USA). Cells were grown in 25-cm^2 primary culture flasks until confluence in minimum essential Eagle's medium (Sigma-Aldrich) with 2 mM GlutaMax, 100 U/ml penicillin, 100 µg/ml streptomycin, and 15% FBS (all from Thermo Fisher Scientific). Cells were incubated at 37°C in 5.5% CO_2 and subcultured by incubation at room temperature in 0.53 mM EDTA in HBSS ($-Mg^{2+}/-Ca^{2+}$) followed by incubation with 0.05% trypsin/0.48 mM EDTA (Thermo Fisher Scientific) at 37°C.

Ca^{2+} imaging

Cells grown on 25-mm glass coverslips were washed and then loaded with 7 µM Fura-2 AM (acetoxymethyl ester, #F1221; Thermo Fisher Scientific) with 0.02% pluronic F-127 (#P3000MP; Thermo Fisher Scientific) for 45 min at 37°C. Cells were washed, mounted in a perfusion chamber, and visualized using a ×40 objective on a Nikon Diaphot microscope (Nikon, Melville, NY, USA) as described (30). Ratiometric measurements were performed by alternating the excitation wavelength from 340 to 380 nm and quantifying emission ≥512 nm with a charge-coupled device camera (All Photon Technologies International, Lawrenceville, NJ, USA). Cells were perfused with isotonic solution containing 105 mM NaCl, 5 mM KCl, 6 mM 4-(2-hydroxyethyl)-1-piperazineethanesulfonic acid, 4 mM Na 4-(2-hydroxyethyl)-1-piperazineethanesulfonic acid, 5 mM $NaHCO_3$, 60 mM mannitol, 5 mM glucose, 1.3 mM $CaCl_2$, and 0.5 mM $MgCl_2$. The ImageJ (NIH; *https://imagej.hin.gov/ij/*) Pseudocolor Look-Up Table (31) was used for displaying images but not for quantification. Because calibration was frequently complicated by cellular manipulations, most of the data were expressed as the ratio of light excited at 340–380 nm ($F_{340/380}$), em >540 nm. However, levels of cytoplasmic calcium were calibrated in some trials as previously reported (32), using 5 µM ionomycin in isotonic (high Ca^{2+}) or Ca^{2+}-free + 5 mM EGTA, both at pH 8.0, based on the equation Ca^{2+} (nM) = K_d*Sf2/Sb2*($R - R_{min}$)/($R_{max} - R$), where K_d = 350 nM, Sf2 is the fluorescence at 380 nm in Ca^{2+}-free and Sb2 in high Ca^{2+} solution, R_{min} is 340/380 nm in Ca^{2+}-free, and R_{max} is 340/380 in high Ca^{2+}. Additional experiments were performed on cells grown to confluence in 96-well black-bottom plates, loaded with Fura-2 AM as previously de-

scribed, and fluorescence was measured in a Fluoroskan Ascent plate reader (Thermo Fisher Scientific) as described in Guha *et al*. (33). Autofluorescence was subtracted from wells when possible.

Microscopy

ARPE-19 cells were grown on glass-bottom dishes for 1 wk with or without CHQ (10 μM) and then treated with U18666A (1 μM) with or without CHQ (10 μM) for 24 h. Autofluorescence and LysoTracker Red were visualized with a Nikon A1R Laser Scanning Confocal Microscope and Nikon NIS-Elements AR (Advanced Research) Software package 3.2 as described in Guha *et al*. (33) at the University of Pennsylvania Live Cell Imaging Core. Cells were incubated with 50 nM LysoTracker Red DND-26 for 30 min at 37°C, washed, and imaged on a warm stage at ex/em 563/590 nm. Autofluorescence was determined from the same fields at ex/em 488/525 nm. Image capture of live cells was completed within 15 min of the end of dye incubation, with settings established first on nontreated cells. For filipin imaging, cells were fixed with 4% formaldehyde, incubated with 50 μg/ml filipin for 1 h in the dark, and fluorescence imaged at ex/em 406/470 nm as above. ImageJ was used to subtract background at a rolling ball radius of 50 pixels, to modulate intensity, and to combine pseudocolored images, with parallel processing for control and experimental images. Images of autofluorescence in ABCA4$^{-/-}$ mice and TRPML1 knockout mice and associated controls were taken in black and white and overlain with orange hot LUT with ImageJ.

PCR analysis

Total RNA was extracted from RPE cells using the RNeasy Mini Kit (Qiagen, Hilden, Germany), and RNA was quantified (Nanodrop; Thermo Fisher Scientific). Total RNA (1 μg) was reverse transcribed using a High Capacity cDNA Kit (Thermo Fisher Scientific). Quantitative PCR (qPCR) was carried out using Power SYBR Green Master Mix with primer pairs mouse TRPML1 (forward, ATGTGGACCCAGCCAATGATACCTT; reverse, TGTCTTCAGCTGGAAGTGGATGGT) and human TRPML1 (forward, TCTTCCAGCACGGAGACAAC; reverse, AACTCGTTCTGCAGCAGGAAGC) using the 7300 Real-Time PCR System. Primers for human PIKfyve were as follows: forward, TGTCTGCGCCTAAAGGTTGTAAA; reverse, TGGATGCCAGATAGCCAATGT. Primers for mouse PIKfyve were as follows: forward, AAGTCTTACCCTCACATGAGCTAGTGA; reverse, ATCAGCTAGCATTCTACCCAAGGT (34). Data were analyzed using the $\Delta\Delta C_t$ approach, with results expressed as fold change in gene expression using an unpaired Student's *t* test as described in Karmakar *et al*. (35).

Materials

ML-SA1 (SML0627; Sigma-Aldrich), MK6-83 (5547; Tocris, Bristol, United Kingdom), thapsigargin (T9033; Sigma-Aldrich), U18666A [(3β)-3-[2-(diethylamino)ethoxy]androst-5-en-17-one hydrochloride, U3633; Sigma-Aldrich], filipin (F9765; Sigma-Aldrich), bafilomycin (B1793; Sigma-Aldrich), glycyl-L-phenylalanine-β-naphthylamide (GPN) (14634; Cayman Chemical, Ann Arbor, MI,

USA), YM201636 (SY-YM201636; Symancis, Temecula, CA, USA), desipramine hydrochloride (sc-200158; Santa Cruz Biotechnology, Dallas, TX, USA), and 2-hydroxypropyl-β-cyclodextrin (12844-35; Sigma-Aldrich) were used in this study.

Statistical analysis

Analysis was performed using SigmaStat (Systat Software, San Jose, CA, USA). Differences between treatments were analyzed using 1-way ANOVA with Holm-Sidak *post hoc* test, rank sum test, or Student's paired Student's *t* test where appropriate. Levels were normalized to the mean value for each experimental set to control for minor daily fluctuations in dye loading. The percent increase was defined as $100[(R_{MLSA1} - R_{BL})/R_{BL}]$ where R_{BL} = 340/380 nm ratio before and R_{MLSA1} after addition of ML-SA1.

RESULTS

ML-SA1 elevates Ca^{2+} in RPE cells

Initial experiments were performed to determine whether activation of TRPML channels raised cytoplasmic calcium in RPE cells. In primary mouse RPE cells loaded with calcium indicator Fura-2 AM, 20 μM of TRPML activator ML-SA1 increased cytoplasmic Ca^{2+} (**Fig. 1*A***). This increase occurred rapidly upon application of ML-SA1, was reversible upon removal of the drug, and was reproducible upon reapplication. Quantification showed that ML-SA1 produced a significant elevation of cytoplasmic Ca^{2+} across multiple trials (Fig. 1*B*). ML-SA1 also raised cytoplasmic calcium levels in hesRPE cells (Fig. 1*C, D*). Although primary mouse and hesRPE cells add validity to the measurement, the use of the ARPE-19 cell line expands the number of manipulations that can be performed. The response to ML-SA1 in ARPE-19 cells was similar, if somewhat more robust (Fig. 1*E–G*).

Release of Ca^{2+} does not involve extracellular influx or endoplasmic reticulum

Additional trials were undertaken to determine whether the increase in cytoplasmic calcium triggered by ML-SA1 reflected the release of lysosomal calcium. The removal of extracellular Ca^{2+} did not diminish the increase in cytoplasmic calcium from mouse RPE cells (**Fig. 2*A***). When multiple responses were quantified, ML-SA1 was shown to induce a similar increase in cytoplasmic Ca^{2+} levels in the presence and absence of extracellular Ca^{2+} (Fig. 2*B*). This implied that the increase in Ca^{2+} levels induced by ML-SA1 in mouse RPE cells was unlikely to be attributed to influx across the plasma membrane. The endoplasmic reticulum (ER) is the largest source of intracellular Ca^{2+}; to determine whether these ER stores contributed to the observed increase in Ca^{2+} levels, cells were treated with 1 μM thapsigargin for 1 h to inhibit the sarco/endoplasmic reticulum Ca^{2+}-ATPase pump and dissipate ER calcium (36). The increase in cytosolic Ca^{2+} levels induced by ML-SA1 in mouse RPE cells was unaffected by thapsigargin (Fig. 2*C, D*), implying that the ER was an unlikely source of the Ca^{2+} increase.

Analogous responses were observed in ARPE-19 cells; neither the removal of extracellular calcium (Fig. 2*E, F*) nor treatment with thapsigargin (Fig. 2*G*) affected the increase in cytoplasmic Ca^{2+} levels induced by ML-SA1. To examine the effect of lysosomal alkalinization on the response to ML-SA1, bafilomycin was used to inhibit the vHATPase proton pump present on lysosomal membranes as bafilomycin was previously found to alkalinize RPE lysosomes by 0.4 pH units (17). Treatment with bafilomycin neither raised baseline cytoplasmic levels nor altered the increase in cytoplasmic Ca^{2+} induced by ML-SA1 (Fig. 2*H*).

Although the prolonged manipulation of cellular Ca^{2+} stores frequently precluded the calibration of absolute Ca^{2+} levels, the response, expressed as a fluorescence ratio, was substantial. Calibration on a subset of responses confirmed that the absolute increase in cytoplasmic calcium triggered by ML-SA1 was robust (Fig. 2*I, J*). Mean levels of cytoplasmic Ca^{2+} were 39.0 ± 1.8 nM; although these baseline levels are lower than those normally found, these measurements were performed in the absence of extracellular Ca^{2+}. Importantly, the addition of 20 μM ML-SA1 raised levels to 50.6 ± 2.0 nM. This represents a mean increase of 30 ± 4%, suggesting the contribution in RPE cells is relevant.

Release of Ca^{2+} linked to lysosomes and TRPML1

Lysosomal involvement was supported by inducing lysosomal rupture with GPN. Hydrolysis of GPN by lysosomal cathepsin C leads to loss of lysosomal membrane integrity and release of lysosomal contents into the cytoplasm (37). Treatment with GPN has been shown to release lysosomal calcium into the cytoplasm (23). RPE cells displayed a substantial rise in cytoplasmic calcium when treated with 200 μM GPN (**Fig. 3*A, B***). Staining of late endosomes/lysosomes with LysoTracker Green was largely eliminated with only 1 min exposure of ARPE-19 cells to GPN (Fig. 3*C, D*). Pretreatment of cells with GPN reduced the magnitude of the response to ML-SA1 (Fig. 3*E, F*), implying that the increase in cytoplasmic Ca^{2+} induced by ML-SA1 was of lysosomal origin.

Additional support for involvement of TRPML channels came from results obtained with a second agonist, MK6-83. Addition of MK6-83 (50 μM) evoked an increase in cytoplasmic calcium in RPE cells (Fig. 3*G, H*). Although the increase induced by MK6-83 was significant, it was less robust and sustained than the increase induced by ML-SA1, consistent with published work (38).

The role of the TRPML1 member of the TRPML family of channels was investigated by examining the effect of ML-SA1 on RPE cells from TRPML1$^{-/-}$ mice. Genotyping confirmed the absence of TRPML1 gene in this line of mice (**Fig. 4*A***). ML-SA1 failed to induce a rise in cytoplasmic calcium in cells from the knockout mice (Fig. 4*B, C*). This lack of Ca^{2+} release was not due to a loss of lysosomal calcium in the TRPML1$^{-/-}$ cells because rupture of the lysosomal membrane with GPN led to a robust increase in cytoplasmic calcium. This lack of response in TRPML1$^{-/-}$ cells strongly suggests that the channel acts as a conduit for calcium efflux after activation of RPE cells by ML-SA1. The increased autofluorescence in RPE whole mounts prepared from TRPML1$^{-/-}$ mice as compared with control [wild-type (WT)] mice supports a role of the channel in RPE physiology (Fig. 4*D, E*). This signal was orders of magnitude less than the fluorescence from cells loaded with the Ca^{2+} indicator Fura-2 AM, however, ensuring that the 2 measurements were independent. There was a moderate increase in autofluorescence in the retina of TRPML1$^{-/-}$ mice (Supplemental Fig. 4).

Although autofluorescence in the RPE cells was brighter than that found elsewhere, we also detected autofluorescence colocalizing with LysoTracker Green in fibroblasts from human patients with MLIV with mutant TRPML1 (Fig. 4*F*). Together, these observations implicate the TRPML1 channel as being largely responsible for the efflux of lysosomal Ca^{2+} into the cytoplasm of RPE cells.

Lipid accumulation impairs lysosomal Ca^{2+} signaling

The experiments described herein strongly suggest that the increase in cytoplasmic calcium accompanying ML-SA1 treatment of RPE cells was linked to the release of lysosomal Ca^{2+} through the TRPML1 channel. Because TRPML1 activity can be impaired by accumulation of lipids (39) and because RPE cells of elderly patients are characterized by the accumulation of lipid peroxidation products (40), we asked whether the accumulation of lysosomal lipid was itself sufficient to impair the activity of TRPML1 in RPE cells.

ARPE-19 cells grown under control conditions showed sporadic autofluorescence, moderate LysoTracker Red signal, and low levels of filipin labeling (**Fig. 5*A***). In contrast, exposure of ARPE-19 cells to 10 μM CHQ for 1 wk increased autofluorescence and the number of lysosomes, as detected with LysoTracker Red (Fig. 5*B*), consistent with impaired degradation and increased biogenesis after CHQ treatment (41). Overlap of autofluorescence and LysoTracker Red indicated that most of the autofluorescence was localized to lysosomes. Treatment with CHQ also increased vesicular binding of filipin, consistent with the increased cholesterol content in those compartments. In cells grown for 6 d in normal medium and then for 1 d in medium containing 1 μM of the intracellular cholesterol transport inhibitor U18666A, the autofluorescence, LysoTracker Red, and filipin signals were higher than in untreated control cells but considerably less than observed in CHQ-treated cells (Fig. 5*C*). Finally, in cells treated with 10 μM CHQ for 6 d and 1 μM U18666A + 10 μM CHQ for 1 d, fluorescence from 3 sources (autofluorescence, LysoTracker Red, and filipin) was enhanced (Fig. 5*D*). The increased autofluorescence was also observed in hesRPE cells treated with CHQ and U18666A (Supplemental Fig. 2). Treatment was also associated with an increase in neutral lipid in lysosomes, as suggested by the overlap between BODIPY 493 and LysoTracker Red fluorescence (Supplemental Fig. 3).

To examine whether autofluorescent lysosomal accumulations were associated with a change in the release of calcium from lysosomes, levels of calcium were measured in control, CHQ-, U18666A-, and CHQ + U18666A–treated ARPE-19 cells. When the response to ML-SA1 was quantified, the increase in cytoplasmic calcium was significantly reduced in cells treated with CHQ and particularly by CHQ + U18666A (Fig. 5*E*). This suggested that cells with the highest number of lysosomes and with the greatest levels of filipin staining and lipofuscin had the lowest levels of calcium efflux through TRPML1.

Several controls were undertaken to confirm that treatment with CHQ and U18666A decreased release of lysosomal Ca^{2+}. First, qPCR indicated that levels of TRPML1 mRNA were not changed in cells treated with CHQ, U18666A, or CHQ + U18666A (Fig. 5*F*). TRPML1 expression showed a slight increase in cells treated with CHQ, although this was not significant. Regardless, this implies that the reduced response to ML-SA1 in treated cells could not be attributed to a reduction in

TRPML1 expression and confirms expression of TRPML1 in both cultured human and fresh mouse RPE cells. Next, the effect of the 4 conditions on the calcium increase after GPN treatment was examined (Fig. 5*G*). GPN induces a near-identical increase in calcium in all cells, implying there was no difference in total calcium stored in lysosomes. Baseline levels of calcium were slightly elevated after CHQ treatment, decreased with U18666A treatment, and revealed no change when both agents were applied (Fig. 5*H*), making the response to ML-SA1 unrelated to the baseline levels. To ensure the autofluorescence did not interfere with the calcium signal, the absolute levels of each were compared; the autofluorescence was <3% of the Fura-2 signal, so the effect on the response is minimal. Finally, to make sure this was not due to a direct effect of CHQ on cytoplasmic calcium, the effect of CHQ alone on baseline calcium levels was measured. CHQ increased levels of cytoplasmic calcium in the short term (Fig. 5*I*), suggesting the reduction in chronically treated cells was not simply a response to CHQ. This implies that reduction of response to ML-SA1 in cells with autofluorescent lysosomal accumulation is not due to changes in lysosomal calcium, to changes in expression of TRPML1, or to direct effects of CHQ.

Reduced response to ML-SA1 in RPE cells from mice with retinal degeneration

The response to TRPML1 activation was examined in RPE cells from mice missing the ABCA4 gene; the ABCA4 gene is mutated in humans with autosomal recessive Stargardt's retinal dystrophy (42). Although the primary defect is in photoreceptor outer segments, RPE cells in ABCA4$^{-/-}$ mice have substantially increased levels of lipofuscin attributed to both bisretinoids and lipids (**Fig. 6*A***; Supplemental Fig. 5) (43, 44). The increase in cytoplasmic calcium induced by ML-SA1 was substantially attenuated in RPE cells from ABCA4$^{-/-}$ mice (Fig. 6*B*). When levels were quantified, ML-SA1 did not induce a significant calcium response in RPE cells from ABCA4$^{-/-}$ mice (Fig. 6*C*).

To probe the decreased Ca^{2+} release in ABCA4$^{-/-}$ cells, several controls were performed, as described above. Levels of TRPML1 mRNA expressed in RPE cells from ABCA4$^{-/-}$ mice were not significantly different from those in WT mice, although there was a trend toward increased expression (Fig. 6*D*). Regardless, the reduced Ca^{2+} response to ML-SA1 could not be explained by a change in TRPML1 expression. In addition, no differences in the levels of lysosomal calcium released by treatment with GPN were found between ABCA4$^{-/-}$ and control RPE cells (Fig. 6*E*); this implies that the levels of calcium stored in lysosomes from the control and mutant cells were the same. Again, the difference in autofluorescence was only 1% of the Fura-2 signal and could not account for this difference in Ca^{2+} release.

Pathways regulating Ca^{2+} release triggered by ML-SA1

Although the release of lysosomal Ca^{2+} was impaired in RPE cells from ABCA4$^{-/-}$ cells and ARPE-19 cells treated with CHQ, the mechanisms linking accumulation to decreased efflux are unclear. The effects of desipramine on the Ca^{2+} response to ML-SA1 were examined to elucidate the consequences of sphingomyelin manipulation, as desipramine is reported to inhibit lysosomal acid sphingomyelinase (45), and mice lacking sphingomyelinase show retinal degeneration (46). Preincubation of ARPE-19 cells with 10 μM desipramine reduced the increase in cytoplasmic Ca^{2+} in response to ML-SA1 (**Fig. 7*A*, *B***). Although this does not prove that sphingomyelin accumula-

tion is responsible for impaired Ca^{2+} efflux in response to ML-SA1, it is consistent with the response to desipramine found in CHO cells, where sphingomyelin was shown to inhibit currents through the channel directly in endolysosome patch clamp recordings (39).

Additional experiments examined the effect of cyclodextrin treatment because U18666A is linked to inhibition of cholesterol trafficking away from the lysosome and the accumulation of lysosomal cholesterol (47). Hydrophobic cyclodextrins extract cholesterol from membranes (48), and cyclodextrins can reduce the pathology associated with lysosomal cholesterol accumulation in Nieman–Pick C disease (49). However, treatment of ARPE-19 cells with 300 μM 2-hydroxypropyl-β-cyclodextrin for 24 h had no effect on the Ca^{2+} increase induced by ML-SA1 in ARPE-19 cells treated with 1 μM U18666A for the previous 24 h (Fig. 7*C*), consistent with findings that cholesterol did not have direct effects on TRPML1 but sphingomyelin did (39). U18666A in the absence of CHQ did not decrease the lysosomal calcium release triggered by ML-SA1. These results suggest that cholesterol is unlikely to be the causal agent.

The most effective endogenous agonist for TRMPL1 identified so far is phosphatidylinositol 3,5-bisphosphate [PI(3,5)P2] (50). To determine whether PI(3,5)P2 influenced the increase in cytoplasmic Ca^{2+} triggered by ML-SA1, cells were pretreated with YM201636. YM201636 inhibits the class III phosphatidylinositol phosphate kinase PIKfyve, which synthesizes PI(3,5)P2 (51). Treatment of ARPE-19 cells with YM201636 reduced the response to ML-SA1 (Fig. 7*A*, *B*), consistent with the ability of PI(3,5)P2 to gate the TRPML1 channel open in RPE cells.

Levels of PIKfyve expression in control and $ABCA4^{-/-}$ mice were examined to determine whether this could contribute to the reduced activity in the mutant cells. Expression of PIKfyve mRNA was reduced by 60% in RPE cells from the $ABCA4^{-/-}$ mouse (Fig. 7*D*). The moderate reduction in expression of PIKfyve from retinal material was not significant. In contrast to the response in the $ABCA4^{-/-}$ mice, levels of PIKfyve mRNA were increased in ARPE-19 cells treated with CHQ + U18666A (protein levels were not measured).

DISCUSSION

The present study identifies lysosomal calcium release through the TRPML1 channel in RPE cells and suggests this release is impaired by lysosomal degradation product accumulation. Evidence to support a role for TRPML1 in the release of lysosomal Ca^{2+} in RPE cells is provided on multiple levels. For example: *1*) RPE cells from WT mice, RPE cells derived from human embryonic stem cells, and the human ARPE-19 cell line show increases in cytoplasmic Ca^{2+} levels after application of the TRPML agonist ML-SA1 in the presence or absence of extracellular Ca^{2+}, ruling out influx from outside as the source of increased cytoplasmic calcium levels; *2*) the increase in cytoplasmic calcium levels triggered by ML-SA1 remained in primary WT mouse RPE and ARPE-19 cells after preincubation with the sarco/endoplasmic reticulum Ca^{2+}-ATPase pump blocker thapsigargin, ruling out the ER as the source of increased cytoplasmic calcium levels; *3*) disruption of lysosomal membranes with GPN raised cytoplasmic calcium levels but eliminated the response to the TRPML1 agonist ML-SA1; this is consistent with the presence of substantial lysosomal calcium stores in RPE cells as the source of the response induced by ML-SA1, although secondary effects of GPN are possible; *4*) ML-SA1 was ineffective against RPE cells from $TRPML1^{-/-}$ mice, although

the release of Ca^{2+} after lysosomal rupture with GPN demonstrated that there was plenty of calcium in the lysosomes of TRPML1$^{-/-}$ RPE cells; *5*) cytoplasmic calcium levels were elevated by a second TRMPL agonist MK6-83. Taken together, these observations suggest that it is highly likely that TRPML1 is a conduit for release of lysosomal Ca^{2+} into the cytoplasm in RPE cells.

One of the notable aspects of the present study is the relative magnitude of increase in cytoplasmic Ca^{2+} induced by ML-SA1. The response was clearly detectable, robust, reproducible, and reversible. It should be emphasized that most of the previous studies performed using ML-SA1 have relied on cells overexpressing the genetically encoded TRPML1 construct to demonstrate lysosomal localization and functionality of the channel (4, 7, 39). In the present study, however, all experiments represent Ca^{2+} release from the endogenous channel. In our study, 20 μM ML-SA1 raised cytoplasmic Ca^{2+} levels by ~30%. In contrast, nontransfected mouse macrophages required a 5-fold increase in ML-SA1 concentration applied to these cells to induce a similar response (39). This implies that the lysosomal Ca^{2+} release may have a relatively high impact on RPE cell signaling, consistent with the critical role of lysosomes in RPE function. Of course, the absolute levels of Ca^{2+} released with 20 μM ML-SA1 are substantially less than those released from the ER by treatment with thapsigargin (52). However, the ability of 20 μM ML-SA1 to induce repeated and sustained release of Ca^{2+} suggests that only a fraction of lysosomal Ca^{2+} is released. Regarding the effects of GPN, the simplest explanation for the dramatic change in LysoTracker Green staining after treatment with GPN is lysosomal rupture. The pH sensitivity of LysoTracker Green, combined with the prolonged effects of GPN on cytoplasmic Ca^{2+} (Fig. 3*A*), suggest there could be a sudden decrease in pH after dissipation of the gradient with accompanying leakage of lysosomal Ca^{2+}.

Decreased lysosomal Ca^{2+} release with accumulations of lipids in lysosomes

The magnitude of lysosomal Ca^{2+} release was reduced in two different models characterized by accumulation of lipids in the lysosomes: in ARPE-19 cells treated with CHQ and U18666A, and in the ABCA4$^{-/-}$ mouse model of recessive Stargardt's disease. The composition of the lysosomal accumulation is quite different because the RPE cells from the ABCA4$^{-/-}$ are characterized by retinoids of photoreceptor origin, such as A2E, that will be missing in the *in vitro* model. However, in both models the reduced release of Ca^{2+} caused by ML-SA1 was not due to a decrease in lysosomal Ca^{2+} stores because Ca^{2+} levels released after lysosomal rupture by GPN were not different from those of controls. Previous reports show a reduced release of Ca^{2+} in response to GPN after treatment with U18666A (3) and in presenilin 1 and 2 double knockout cells (53), suggesting a reduction in total lysosomal Ca^{2+} levels, but that was not found in the present study. Treatment with CHQ stimulates lysosomal biogenesis (54), and our measurements may reflect less Ca^{2+} release from more lysosomes. However, this would not explain why release was less in cells treated with ML-SA1 and not GPN. The reduction in the amount of Ca^{2+} released was not due to decreased expression of TRPML1. In fact, expression of TRPML1 trended upward in both models, consistent with nuclear delivery of TRPML1 transcription factor TFEB upon lysosomal compromise (55). Although this increase in TRPML1 expression was not significant in either model, it is not consistent with a reduced response to ML-SA1. The reduction in PIKfyve in RPE cells from ABCA4$^{-/-}$ mice could explain the reduced release in these cells because the product of the enzyme, PI(3,5)P2, is an endogenous agonist for TRPML1 (50), although the increase in PIKfyve levels in

the *in vitro* model argues against this. The mechanisms could differ in the 2 models given the differences in their lipofuscin composition. Further analysis is needed to identify the component responsible for the reduced response to ML-SA1 in both of these models.

Ca^{2+} signaling makes a key contribution to several important functions of RPE cells, including ion and fluid transport, phagocytosis of photoreceptor outer segments, and secretion (56, 57). The TRPML1 channel has recently been implicated in multiple cellular functions, including phagocytosis (58), secretion (59), control of organelle motility (6), regulation of transcription factor TFEB (7), response to cellular starvation (8), and control of lysosome size (60). Although the degree to which TRPML1 influences these functions in RPE cells remains to be determined, mutations in TRPML1 lead to MLIV, a severe lysosomal storage disorder (11, 61), and both human patients with MLIV and $TRPML1^{-/-}$ mice exhibit retinal degeneration (15). Of particular relevance is the ability of TRPML1 activation to target lysosomal storage diseases due to mutations in distinct enzymes, such as Niemann–Pick C (39), or the role of TRPML1 in clearing lysosomal degradation product accumulation in several different models of lysosomal storage disease (62, 63). Whether defective lysosomal Ca^{2+} signaling contributes to lysosomal accumulation in RPE cells and how the newly identified acid Ca/H exchanger (64, 65) contributes to this release remain to be determined.

Portions of this work were previously presented in abstract form (66, 67).

Supplementary Material

This article includes supplemental data. Please visit *http://www.fasebj.org* to obtain this information.

ACKNOWLEDGMENTS

The authors thank Lincoln Johnson (Laboratory for Stem Cell Biology and Engineering, Neuroscience Research Institute, University of California, Santa Barbara, Santa Barbara, CA, USA) for the generous donation of hesRPE cells. This work was supported by U.S. National Institutes of Health (NIH) National Eye Institute Grants EY015537 and EY013434 and Core Grant EY001583 (to C.H.M.) and EY007361 (to S.J.F.), by NIH National Center for Advancing Translational Science Grant U54 TR001358 to SUNY–University at Buffalo (S.J.F.), by the Jody Sack Fund (to W.L.), and by an Unrestricted Grant from Research to Prevent Blindness to the Department of Ophthalmology, SUNY–University at Buffalo, from Research to Prevent Blindness (to S.J.F.). The opinions expressed herein do not necessarily reflect those of the Veterans Administration or the U.S. Government. The authors declare no conflicts of interest.

Glossary

ABCA4	ATP-binding cassette, subfamily A, member 4
CHQ	chloroquine
ER	endoplasmic reticulum
FBS	fetal bovine serum
GPN	glycyl-L-phenylalanine-β-naphthylamide
hesRPE cells	human embryonic stem cell–derived RPE
MCOLN1	mucolipin 1
MLIV	mucolipidosis type IV
qPCR	quantitative PCR
RPE	retinal pigmented epithelium
TFEB	transcription factor EB
TRPML1	transient receptor potential cation channel mucolipin 1
WT	wild type

Footnotes

This article includes supplemental data. Please visit http://www.fasebj.org to obtain this information.

AUTHOR CONTRIBUTIONS

N. M. Gomez, K. Kiselyov, and C. H. Mitchell designed the research; N. M. Gomez, C. H. Mitchell, and K. E. Campagno wrote and/or helped edit the paper; N. M. Gomez, W. Lu, and J. C. Lim performed the experiments; and Y. Grishchuk, B. A. Pfeffer, and S. J. Fliesler contributed new reagents or analytic tools and helped edit the paper.

REFERENCES

1. Christensen K. A., Myers J. T., Swanson J. A. (2002) pH-dependent regulation of lysosomal calcium in macrophages. *J. Cell Sci.* 115, 599–607 [PubMed: 11861766]

2. Xu H., Ren D. (2015) Lysosomal physiology. *Annu. Rev. Physiol.* 77, 57–80 [PMCID: PMC4524569] [PubMed: 25668017]

3. Lloyd-Evans E., Morgan A. J., He X., Smith D. A., Elliot-Smith E., Sillence D. J., Churchill G. C., Schuchman E. H., Galione A., Platt F. M. (2008) Niemann-Pick disease type C1 is a sphingosine storage disease that causes deregulation of lysosomal calcium. *Nat. Med.* 14, 1247–1255 [PubMed: 18953351]

4. Cheng X., Zhang X., Gao Q., Ali Samie M., Azar M., Tsang W. L., Dong L., Sahoo N., Li X., Zhuo Y., Garrity A. G., Wang X., Ferrer M., Dowling J., Xu L., Han R., Xu H. (2014) The intracellular Ca^{2+} channel MCOLN1 is required for sarcolemma repair to prevent muscular dystrophy. *Nat. Med.* 20, 1187–1192 [PMCID: PMC4192061] [PubMed: 25216637]

5. Al-Bari M. A. (2015) Chloroquine analogues in drug discovery: new directions of uses, mechanisms of actions and toxic manifestations from malaria to multifarious diseases. *J. Antimicrob. Chemother.* 70, 1608–1621 [PMCID: PMC7537707] [PubMed: 25693996]

6. Li X., Rydzewski N., Hider A., Zhang X., Yang J., Wang W., Gao Q., Cheng X., Xu H. (2016) A molecular mechanism to regulate lysosome motility for lysosome positioning and tubulation. *Nat. Cell Biol.* 18, 404–417 [PMCID: PMC4871318] [PubMed: 26950892]

7. Medina D. L., Di Paola S., Peluso I., Armani A., De Stefani D., Venditti R., Montefusco S., Scotto-Rosato A., Prezioso C., Forrester A., Settembre C., Wang W., Gao Q., Xu H., Sandri M., Rizzuto R., De Matteis M. A., Ballabio A. (2015) Lysosomal calcium signalling regulates autophagy through calcineurin and TFEB. *Nat. Cell Biol.* 17, 288–299 [PMCID: PMC4801004] [PubMed: 25720963]

8. Wang W., Gao Q., Yang M., Zhang X., Yu L., Lawas M., Li X., Bryant-Genevier M., Southall N. T., Marugan J., Ferrer M., Xu H. (2015) Up-regulation of lysosomal TRPML1 channels is essential for lysosomal adaptation to nutrient starvation. *Proc. Natl. Acad. Sci. USA* 112, E1373–E1381 [PMCID: PMC4371935] [PubMed: 25733853]

9. Zhang X., Cheng X., Yu L., Yang J., Calvo R., Patnaik S., Hu X., Gao Q., Yang M., Lawas M., Delling M., Marugan J., Ferrer M., Xu H. (2016) MCOLN1 is a ROS sensor in lysosomes that regulates autophagy. *Nat. Commun.* 7, 12109. [PMCID: PMC4931332] [PubMed: 27357649]

10. Venkatachalam K., Hofmann T., Montell C. (2006) Lysosomal localization of TRPML3 depends on TRPML2 and the mucolipidosis-associated protein TRPML1. *J. Biol. Chem.* 281, 17517–17527 [PMCID: PMC4196876] [PubMed: 16606612]

11. Sun M., Goldin E., Stahl S., Falardeau J. L., Kennedy J. C., Acierno J. S. Jr., Bove C., Kaneski C. R., Nagle J., Bromley M. C., Colman M., Schiffmann R., Slaugenhaupt S. A. (2000) Mucolipidosis type IV is caused by mutations in a gene encoding a novel transient receptor potential channel. *Hum. Mol. Genet.* 9, 2471–2478 [PubMed: 11030752]

12. Goldin E., Caruso R. C., Benko W., Kaneski C. R., Stahl S., Schiffmann R. (2008) Isolated ocular disease is associated with decreased mucolipin-1 channel conductance. *Invest. Ophthalmol. Vis. Sci.* 49, 3134–3142 [PMCID: PMC5267708] [PubMed: 18326692]

13. Venugopal B., Browning M. F., Curcio-Morelli C., Varro A., Michaud N., Nanthakumar N., Walkley S. U., Pickel J., Slaugenhaupt S. A. (2007) Neurologic, gastric, and opthalmologic pathologies in a murine model of mucolipidosis type IV. *Am. J. Hum. Genet.* 81, 1070–1083 [PMCID: PMC2265643] [PubMed: 17924347]

14. Bach G. (2001) Mucolipidosis type IV. *Mol. Genet. Metab.* 73, 197–203 [PubMed: 11461186]

15. Grishchuk Y., Stember K. G., Matsunaga A., Olivares A. M., Cruz N. M., King V. E., Humphrey D. M., Wang S. L., Muzikansky A., Betensky R. A., Thoreson W. B., Haider N., Slaugenhaupt S. A. (2016) Retinal dystrophy and optic nerve pathology in the mouse model of mucolipidosis IV. *Am. J. Pathol.* 186, 199–209 [PMCID: PMC4715222] [PubMed: 26608452]

16. LaVail M. M. (1976) Rod outer segment disk shedding in rat retina: relationship to cyclic lighting. *Science* 194, 1071–1074 [PubMed: 982063]

17. Liu J., Lu W., Reigada D., Nguyen J., Laties A. M., Mitchell C. H. (2008) Restoration of lysosomal pH in RPE cells from cultured human and ABCA4(-/-) mice: pharmacologic approaches and functional recovery. *Invest. Ophthalmol. Vis. Sci.* 49, 772–780 [PMCID: PMC2279299] [PubMed: 18235027]

18. Weng J., Mata N. L., Azarian S. M., Tzekov R. T., Birch D. G., Travis G. H. (1999) Insights into the function of Rim protein in photoreceptors and etiology of Stargardt's disease from the phenotype in abcr knockout mice. *Cell* 98, 13–23 [PubMed: 10412977]

19. Guha S., Liu J., Baltazar G., Laties A. M., Mitchell C. H. (2014) Rescue of compromised lysosomes enhances degradation of photoreceptor outer segments and reduces lipofuscin-like autofluorescence in retinal pigmented epithelial cells. *Adv. Exp. Med. Biol.* 801, 105–111 [PMCID: PMC4163923] [PubMed: 24664687]

20. Kellner U., Kellner S., Weinitz S. (2008) Chloroquine retinopathy: lipofuscin- and melanin-related fundus autofluorescence, optical coherence tomography and multifocal electroretinography. *Doc. Ophthalmol.* 116, 119–127 [PubMed: 18080820]

21. Mitter S. K., Song C., Qi X., Mao H., Rao H., Akin D., Lewin A., Grant M., Dunn W. Jr., Ding J., Bowes Rickman C., Boulton M. (2014) Dysregulated autophagy in the RPE is associated with increased susceptibility to oxidative stress and AMD. *Autophagy* 10, 1989–2005 [PMCID: PMC4502658] [PubMed: 25484094]

22. Frost L. S., Mitchell C. H., Boesze-Battaglia K. (2014) Autophagy in the eye: implications for ocular cell health. *Exp. Eye Res.* 124, 56–66 [PMCID: PMC4156154] [PubMed: 24810222]

23. Soyombo A. A., Tjon-Kon-Sang S., Rbaibi Y., Bashllari E., Bisceglia J., Muallem S., Kiselyov K. (2006) TRP-ML1 regulates lysosomal pH and acidic lysosomal lipid hydrolytic activity. *J. Biol. Chem.* 281, 7294–7301 [PubMed: 16361256]

24. Guha S., Baltazar G. C., Coffey E. E., Tu L.-A., Lim J. C., Beckel J. M., Eysteinsson T., Lu W., O'Brien-Jenkins A., Patel S., Laties A. M., Mitchell C. H. (2013) Lysosomal alkalinization, lipid oxidation, impaired autophagy and reduced phagosome clearance triggered by P2X7 receptor activation in retinal pigmented epithelial cells. *FASEB J.* 27, 4500–4509 [PMCID: PMC3804754] [PubMed: 23964074]

25. Kim S. R., Fishkin N., Kong J., Nakanishi K., Allikmets R., Sparrow J. R. (2004) Rpe65 Leu450Met variant is associated with reduced levels of the retinal pigment epithelium lipofuscin fluorophores A2E and iso-A2E. *Proc. Natl. Acad. Sci. USA* 101, 11668–11672 [PMCID: PMC511036] [PubMed: 15277666]

26. Mattapallil M. J., Wawrousek E. F., Chan C. C., Zhao H., Roychoudhury J., Ferguson T. A., Caspi R. R. (2012) The Rd8 mutation of the Crb1 gene is present in vendor lines of C57BL/6N mice and embryonic stem cells, and confounds ocular induced mutant phenotypes. *Invest. Ophthalmol. Vis. Sci.* 53, 2921–2927 [PMCID: PMC3376073] [PubMed: 22447858]

27. Rowland T. J., Blaschke A. J., Buchholz D. E., Hikita S. T., Johnson L. V., Clegg D. O. (2013) Differentiation of human pluripotent stem cells to retinal pigmented epithelium in defined conditions using purified extracellular matrix proteins. *J. Tissue Eng. Regen. Med.* 7, 642–653 [PubMed: 22514096]

28. Pfeffer B. A. (1991) Improved methodology for cell culture of human and monkey retinal pigment epithelium. *Prog. Retinal Res.* 10, 251–291

29. Reigada D., Lu W., Zhang X., Friedman C., Pendrak K., McGlinn A., Stone R. A., Laties A. M., Mitchell C. H. (2005) Degradation of extracellular ATP by the retinal pigment epithelium. *Am. J. Physiol. Cell Physiol.* 289, C617–C624 [PubMed: 15857904]

30. Zeiger U., Mitchell C. H., Khurana T. S. (2010) Superior calcium homeostasis of extraocular muscles. *Exp. Eye Res.* 91, 613–622 [PMCID: PMC4086352] [PubMed: 20696159]

31. Schneider C. A., Rasband W. S., Eliceiri K. W. (2012) NIH Image to ImageJ: 25 years of image analysis. *Nat. Methods* 9, 671–675 [PMCID: PMC5554542] [PubMed: 22930834]

32. Zhang M., Hu H., Zhang X., Lu W., Lim J., Eysteinsson T., Jacobson K. A., Laties A. M., Mitchell C. H. (2010) The A3 adenosine receptor attenuates the calcium rise triggered by NMDA receptors in retinal ganglion cells. *Neurochem. Int.* 56, 35–41 [PMCID: PMC2814940] [PubMed: 19723551]

33. Guha S., Baltazar G. C., Tu L. A., Liu J., Lim J. C., Lu W., Argall A., Boesze-Battaglia K., Laties A. M., Mitchell C. H. (2012) Stimulation of the D5 dopamine receptor acidifies the lysosomal pH of retinal pigmented epithelial cells and decreases accumulation of autofluorescent photoreceptor debris. *J. Neurochem.* 122, 823–833 [PMCID: PMC3408960] [PubMed: 22639870]

34. Kawasaki T., Takemura N., Standley D. M., Akira S., Kawai T. (2013) The second messenger phosphatidylinositol-5-phosphate facilitates antiviral innate immune signaling. *Cell Host Microbe* 14, 148–158 [PubMed: 23954154]

35. Karmakar M., Katsnelson M., Malak H. A., Greene N. G., Howell S. J., Hise A. G., Camilli A., Kadioglu A., Dubyak G. R., Pearlman E. (2015) Neutrophil IL-1β processing induced by pneumolysin is mediated by the NLRP3/ASC inflammasome and caspase-1 activation and is dependent on K+ efflux. *J. Immunol.* 194, 1763–1775 [PMCID: PMC4369676] [PubMed: 25609842]

36. Lytton J., Westlin M., Hanley M. R. (1991) Thapsigargin inhibits the sarcoplasmic or endoplasmic reticulum Ca-ATPase family of calcium pumps. *J. Biol. Chem.* 266, 17067–17071 [PubMed: 1832668]

37. Jadot M., Colmant C., Wattiaux-De Coninck S., Wattiaux R. (1984) Intralysosomal hydrolysis of glycyl-L-phenylalanine 2-naphthylamide. *Biochem. J.* 219, 965–970 [PMCID: PMC1153569] [PubMed: 6743255]

38. Chen C.-C., Keller M., Hess M., Schiffmann R., Urban N., Wolfgardt A., Schaefer M., Bracher F., Biel M., Wahl-Schott C., Grimm C. (2014) A small molecule restores function to TRPML1 mutant isoforms responsible for mucolipidosis type IV. *Nat. Commun.* 5, 4681. [PubMed: 25119295]

39. Shen D., Wang X., Li X., Zhang X., Yao Z., Dibble S., Dong X. P., Yu T., Lieberman A. P., Showalter H. D., Xu H. (2012) Lipid storage disorders block lysosomal trafficking by inhibiting a TRP channel and lysosomal calcium release. *Nat. Commun.* 3, 731. [PMCID: PMC3347486] [PubMed: 22415822]

40. Sparrow J. R., Boulton M. (2005) RPE lipofuscin and its role in retinal pathobiology. *Exp. Eye Res.* 80, 595–606 [PubMed: 15862166]

41. Emanuel R., Sergin I., Bhattacharya S., Turner J., Epelman S., Settembre C., Diwan A., Ballabio A., Razani B. (2014) Induction of lysosomal biogenesis in atherosclerotic macrophages can rescue lipid-induced lysosomal dysfunction and downstream sequelae. *Arterioscler. Thromb. Vasc. Biol.* 34, 1942–1952 [PMCID: PMC4140993] [PubMed: 25060788]

42. Allikmets R., Shroyer N. F., Singh N., Seddon J. M., Lewis R. A., Bernstein P. S., Peiffer A., Zabriskie N. A., Li Y., Hutchinson A., Dean M., Lupski J. R., Leppert M. (1997) Mutation of the Stargardt disease gene (ABCR) in age-related macular degeneration. *Science* 277, 1805–1807 [PubMed: 9295268]

43. Sparrow J. R., Dowling J. E., Bok D. (2013) Understanding RPE lipofuscin. *Invest. Ophthalmol. Vis. Sci.* 54, 8325–8326 [PMCID: PMC4830350] [PubMed: 24356235]

44. Toops K. A., Tan L. X., Jiang Z., Radu R. A., Lakkaraju A. (2015) Cholesterol-mediated activation of acid sphingomyelinase disrupts autophagy in the retinal pigment epithelium. *Mol. Biol. Cell* 26, 1–14 [PMCID: PMC4279221] [PubMed: 25378587]

45. Kölzer M., Werth N., Sandhoff K. (2004) Interactions of acid sphingomyelinase and lipid bilayers in the presence of the tricyclic antidepressant desipramine. *FEBS Lett.* 559, 96–98 [PubMed: 14960314]

46. Wu B. X., Fan J., Boyer N. P., Jenkins R. W., Koutalos Y., Hannun Y. A., Crosson C. E. (2015) Lack of acid sphingomyelinase induces age-related retinal degeneration. *PLoS One* 10, e0133032. [PMCID: PMC4500403] [PubMed: 26168297]

47. Cenedella R. J. (2009) Cholesterol synthesis inhibitor U18666A and the role of sterol metabolism and trafficking in numerous pathophysiological processes. *Lipids* 44, 477–487 [PubMed: 19440746]

48. Zidovetzki R., Levitan I. (2007) Use of cyclodextrins to manipulate plasma membrane cholesterol content: evidence, misconceptions and control strategies. *Biochim. Biophys. Acta* 1768, 1311–1324 [PMCID: PMC1948080] [PubMed: 17493580]

49. Davidson C. D., Ali N. F., Micsenyi M. C., Stephney G., Renault S., Dobrenis K., Ory D. S., Vanier M. T., Walkley S. U. (2009) Chronic cyclodextrin treatment of murine Niemann-Pick C disease ameliorates neuronal cholesterol and glycosphingolipid storage and disease progression. *PLoS One* 4, e6951. [PMCID: PMC2736622] [PubMed: 19750228]

50. Dong X. P., Shen D., Wang X., Dawson T., Li X., Zhang Q., Cheng X., Zhang Y., Weisman L. S., Delling M., Xu H. (2010) PI(3,5)P(2) controls membrane trafficking by direct activation of mucolipin Ca(2+) release channels in the endolysosome. *Nat. Commun.* 1, 38. [PMCID: PMC2928581] [PubMed: 20802798]

51. Jefferies H. B. J., Cooke F. T., Jat P., Boucheron C., Koizumi T., Hayakawa M., Kaizawa H., Ohishi T., Workman P., Waterfield M. D., Parker P. J. (2008) A selective PIKfyve inhibitor blocks PtdIns(3,5)P(2) production and disrupts endomembrane transport and retroviral budding. *EMBO Rep.* 9, 164–170 [PMCID: PMC2246419] [PubMed: 18188180]

52. Gómez N. M., Tamm E. R., Strauβ O. (2013) Role of bestrophin-1 in store-operated calcium entry in retinal pigment epithelium. *Pflugers Arch.* 465, 481–495 [PubMed: 23207577]

53. Coen K., Flannagan R. S., Baron S., Carraro-Lacroix L. R., Wang D., Vermeire W., Michiels C., Munck S., Baert V., Sugita S., Wuytack F., Hiesinger P. R., Grinstein S., Annaert W. (2012) Lysosomal calcium homeostasis defects, not proton pump defects, cause endo-lysosomal dysfunction in PSEN-deficient cells. *J. Cell Biol.* 198, 23–35 [PMCID: PMC3392942] [PubMed: 22753898]

54. Ma X., Godar R. J., Liu H., Diwan A. (2012) Enhancing lysosome biogenesis attenuates BNIP3-induced cardiomyocyte death. *Autophagy* 8, 297–309 [PMCID: PMC3337840] [PubMed: 22302006]

55. Settembre C., Zoncu R., Medina D. L., Vetrini F., Erdin S., Erdin S., Huynh T., Ferron M., Karsenty G., Vellard M. C., Facchinetti V., Sabatini D. M., Ballabio A. (2012) A lysosome-to-nucleus signalling mechanism senses and regulates the lysosome via mTOR and TFEB. *EMBO J.* 31, 1095–1108 [PMCID: PMC3298007] [PubMed: 22343943]

56. Wimmers S., Karl M. O., Strauss O. (2007) Ion channels in the RPE. *Prog. Retin. Eye Res.* 26, 263–301 [PubMed: 17258931]

57. Strauß O., Reichhart N., Gomez N. M., Müller C. (2016) Contribution of ion channels in calcium signaling regulating phagocytosis: MaxiK, Cav1.3 and Bestrophin-1. *Adv. Exp. Med. Biol.* 854, 739–744 [PubMed: 26427483]

58. Samie M., Wang X., Zhang X., Goschka A., Li X., Cheng X., Gregg E., Azar M., Zhuo Y., Garrity A. G., Gao Q., Slaugenhaupt S., Pickel J., Zolov S. N., Weisman L. S., Lenk G. M., Titus S., Bryant-Genevier M., Southall N., Juan M., Ferrer M., Xu H. (2013) A TRP channel in the lysosome regulates large particle phagocytosis via focal exocytosis. *Dev. Cell* 26, 511–524 [PMCID: PMC3794471] [PubMed: 23993788]

59. Chandra M., Zhou H., Li Q., Muallem S., Hofmann S. L., Soyombo A. A. (2011) A role for the Ca2+ channel TRPML1 in gastric acid secretion, based on analysis of knockout mice. *Gastroenterology* 140, 857–867 [PMCID: PMC3057336] [PubMed: 21111738]

60. Cao Q., Yang Y., Zhong X. Z., Dong X.-P. (2017) The lysosomal Ca(2+) release channel TRPML1 regulates lysosome size by activating calmodulin. *J. Biol. Chem.* 292, 8424–8435 [PMCID: PMC5437247] [PubMed: 28360104]

61. Bargal R., Avidan N., Olender T., Ben Asher E., Zeigler M., Raas-Rothschild A., Frumkin A., Ben-Yoseph O., Friedlender Y., Lancet D., Bach G. (2001) Mucolipidosis type IV: novel MCOLN1 mutations in Jewish and non-Jewish patients and the frequency of the disease in the Ashkenazi Jewish population. *Hum. Mutat.* 17, 397–402 [PubMed: 11317355]

62. Weiss N. (2012) Cross-talk between TRPML1 channel, lipids and lysosomal storage diseases. *Commun. Integr. Biol.* 5, 111–113 [PMCID: PMC3376041] [PubMed: 22808310]

63. Medina D. L., Fraldi A., Bouche V., Annunziata F., Mansueto G., Spampanato C., Puri C., Pignata A., Martina J. A., Sardiello M., Palmieri M., Polishchuk R., Puertollano R., Ballabio A. (2011) Transcriptional activation of lysosomal exocytosis promotes cellular clearance. *Dev. Cell* 21, 421–430 [PMCID: PMC3173716] [PubMed: 21889421]

64. Melchionda M., Pittman J. K., Mayor R., Patel S. (2016) Ca2+/H+ exchange by acidic organelles regulates cell migration in vivo. *J. Cell Biol.* 212, 803–813 [PMCID: PMC4810305] [PubMed: 27002171]

65. Lloyd-Evans E. (2016) On the move, lysosomal CAX drives Ca2+ transport and motility. *J. Cell Biol.* 212, 755–757 [PMCID: PMC4810312] [PubMed: 27022089]

66. Gómez N. M., Lu W., Lim J., Laties A., Kiselyov K., Mitchell C. H. (2016) Impaired lysosomal calcium signaling in RPE cells with an in vitro model of chloroquine retinopathy. *Invest. Ophthalmol. Vis. Sci.* 57, 6050

67. Gómez N. M., Lu W., Lim J. C., Laties A. M., Kiselyov K., Mitchell C. H. (2015) Lysosomal stress impairs calcium signaling by TRPML in RPE cells. *Invest. Ophthalmol. Vis. Sci.* 56, 5437

Figures and Tables

Figure 1.

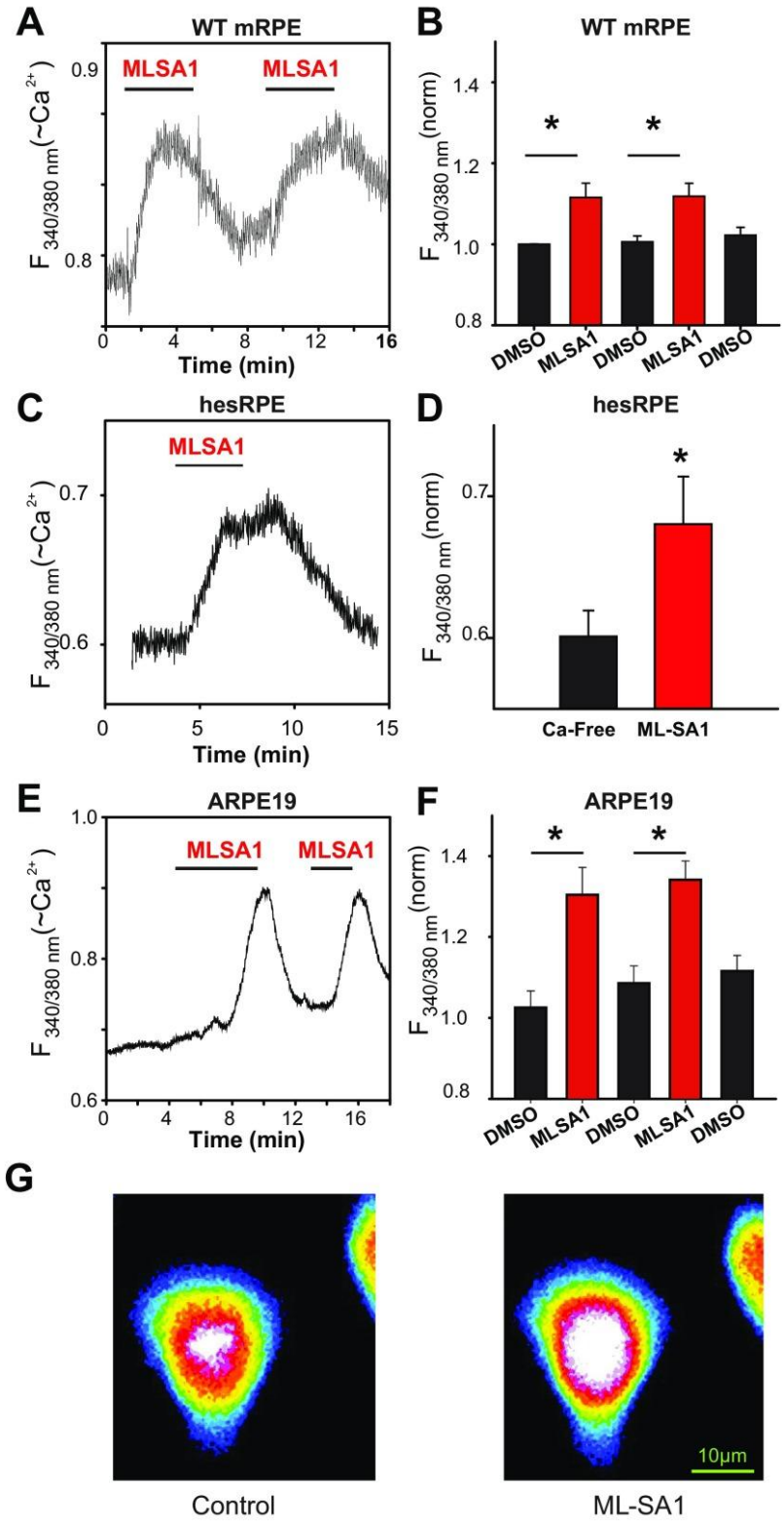

Response to ML-SA1 in various RPE cells. *A*) Representative trace from a WT mouse RPE (mRPE) cell loaded with Fura-2 showing the increase in the cytoplasmic calcium signal in response to 20 μM ML-SA1. The response was reversible and repeatable. Data are expressed as the ratio of light excited at 340 *vs.* 380 nm, em >520 nm (referred to as $F_{340/380}$), indicative of cytoplasmic calcium in cells loaded with Fura-2. *B*) Quantification of the increase in $F_{340/380}$ accompanying application and reapplication of 20 μM ML-SA1 in mRPE compared with control levels in DMSO vehicle. **P* = 0.012, first application; *P* = 0.013, second application (*n* = 5). *C*) Representative trace from an RPE cell derived from a hesRPE loaded with Fura-2

showing the increase in $F_{340/380}$ in response to 20 μM ML-SA1. *D*) Quantification of the increase in $F_{340/380}$ accompanying 20 μM ML-SA1 in hesRPE cells. **P* = 0.042 (*n* = 5). *E*) Representative trace from a human ARPE-19 cell loaded with Fura-2 showing the increase in $F_{340/380}$ in response to 20 μM ML-SA1. The increase was more robust than the mRPE but was quantitatively similar. *F*) Quantification of the increase in $F_{340/380}$ accompanying 20 μM ML-SA1 in ARPE-19 cells. **P* < 0.001, first application; *P* = 0.003, second application (*n* = 17). *G*) Representative images illustrating the increase in cytoplasmic calcium after the addition of ML-SA1 to ARPE-19 cells. Pseudocolored images represent changes in 340/380 nm intensity, with white representing increased Ca^{2+}. Experiments above were performed with 1.3 mM extracellular calcium except *C* and *D*, which used Ca^{2+}-free solution. Analysis was determined using ANOVA and Holm-Sidak *post hoc* test, with $F_{340/380}$ normalized to initial level for each trial in *B* and *F*.

Figure 2.

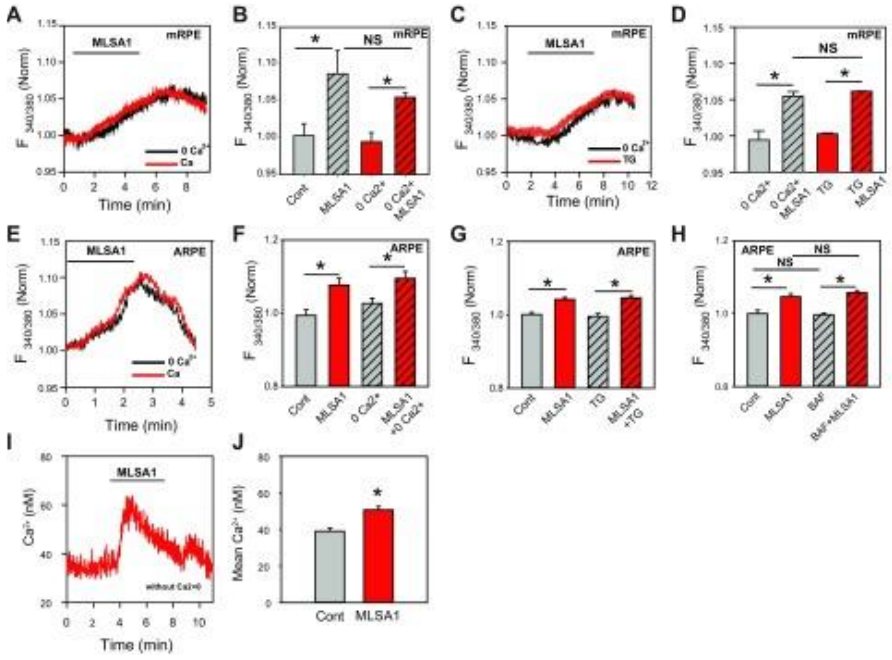

Lysosomal source of calcium in the RPE. *A*) Overlay of traces from mouse RPE exposed to 20 μM ML-SA1 in the presence and absence of extracellular Ca^{2+}. Data are expressed as the ratio of light excited at 340 nm *vs.* 380 nm, em >520 nm (referred to as $F_{340/380}$), indicative of cytoplasm calcium in cells loaded with Fura-2. *B*) Quantification of the increase with and without extracellular calcium. *P* < 0.05 (*n* = 3). NS, no significant difference. *C*) Overlay of traces from mouse RPE exposed to 20 μM ML-SA1 in the presence and absence of thapsigargin in calcium-free solution. *D*) Quantification of the increase with and without thapsigargin in extracellular calcium-free solution. **P* < 0.01. *E*) Overlay of $F_{340/380}$ response to 20 μM ML-SA1 in the presence and absence of calcium from a typical ARPE-19 cell line. *F*) Quantification of the $F_{340/380}$ response to 20 μM ML-SA1 in the presence and absence of calcium from trials shown in *E*. **P* < 0.05 (*n* = 25). *G*) Quantification of ARPE-19 cells with and without 1 h pretreatment with 1 μM thapsigargin. **P* < 0.001 (*n* = 40). *H*) Treatment of ARPE-19 cells with bafilomycin (BAF) (1 μM for 1 h at 37°C) altered neither baseline Ca^{2+} levels nor the increase in cytoplasmic calcium triggered by ML-SA1. **P* < 0.001 (*n* = 10), representative or 3 separate trials. *I*) Sample of an ARPE-19 cell calibrated to illustrate the magnitude of the response to MLSA-1 (*J*). Mean responses in calibrated cells. *P* < 0.001 (*n* = 63).

Figure 3.

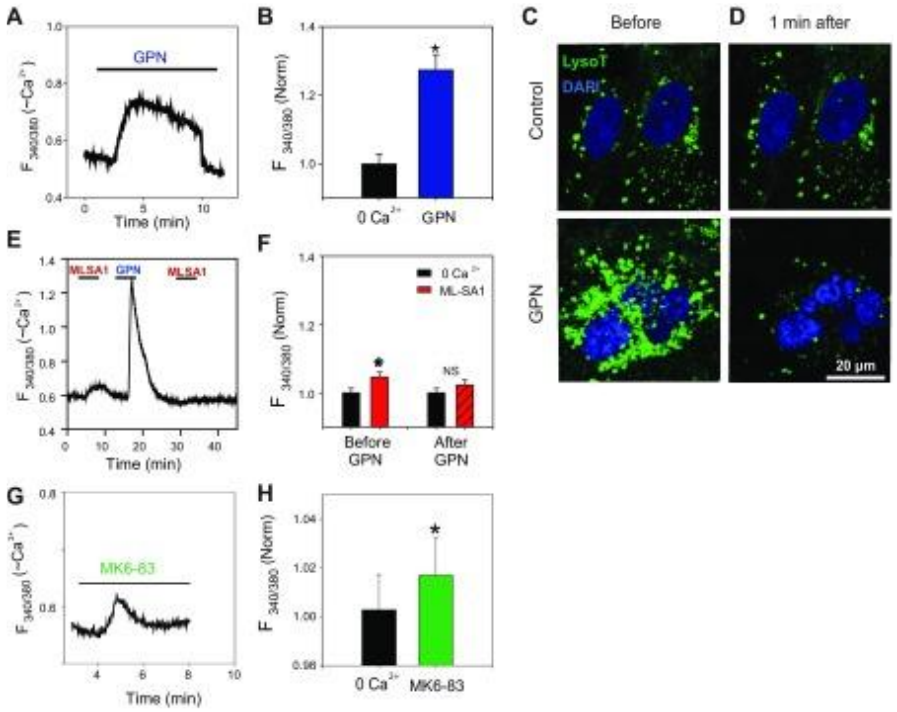

Confirmation of the lysosomal source of calcium in the RPE. *A*). Representative trace from ARPE-19 cells in Ca^{2+}-free solution with the addition of 200 µM GPN. Data are expressed as the ratio of light excited at 340 *vs.* 380 nm, em >520 nm (referred to as $F_{340/380}$), indicative of cytoplasmic calcium in cells loaded with Fura-2. *B*) Mean increase in $F_{340/380}$ observed with GPN. *P < 0.001, Mann-Whitney rank sum test (n = 8). ARPE-19 cells were loaded with LysoTracker Green before (*C*) and 1 min after (*D*) addition of either control (top) or 200 µM GPN, showing decrease in LysoTracker Green staining with GPN. *E*) GPN reduces the ML-SA1 response. Representative trace indicating the increase in calcium induced by 20 µM ML-SA1 is reduced after lysosomal membrane permeabilization by GPN. *F*) Quantification of the increase in calcium invoked by 20 µM ML-SA1 before and after release of lysosomal Ca^{2+} by GPN. *P = 0.025, Holm-Sidak test (n = 29). NS, not significant. *G*) Representative trace demonstrating the ability of 50 µM TRPML agonist MK6-83 to elevate cytoplasmic calcium. *H*) Quantification of the increase in calcium invoked by 50 µM MK6-83. P = 0.002, paired Student's t test (n = 11).

Figure 4.

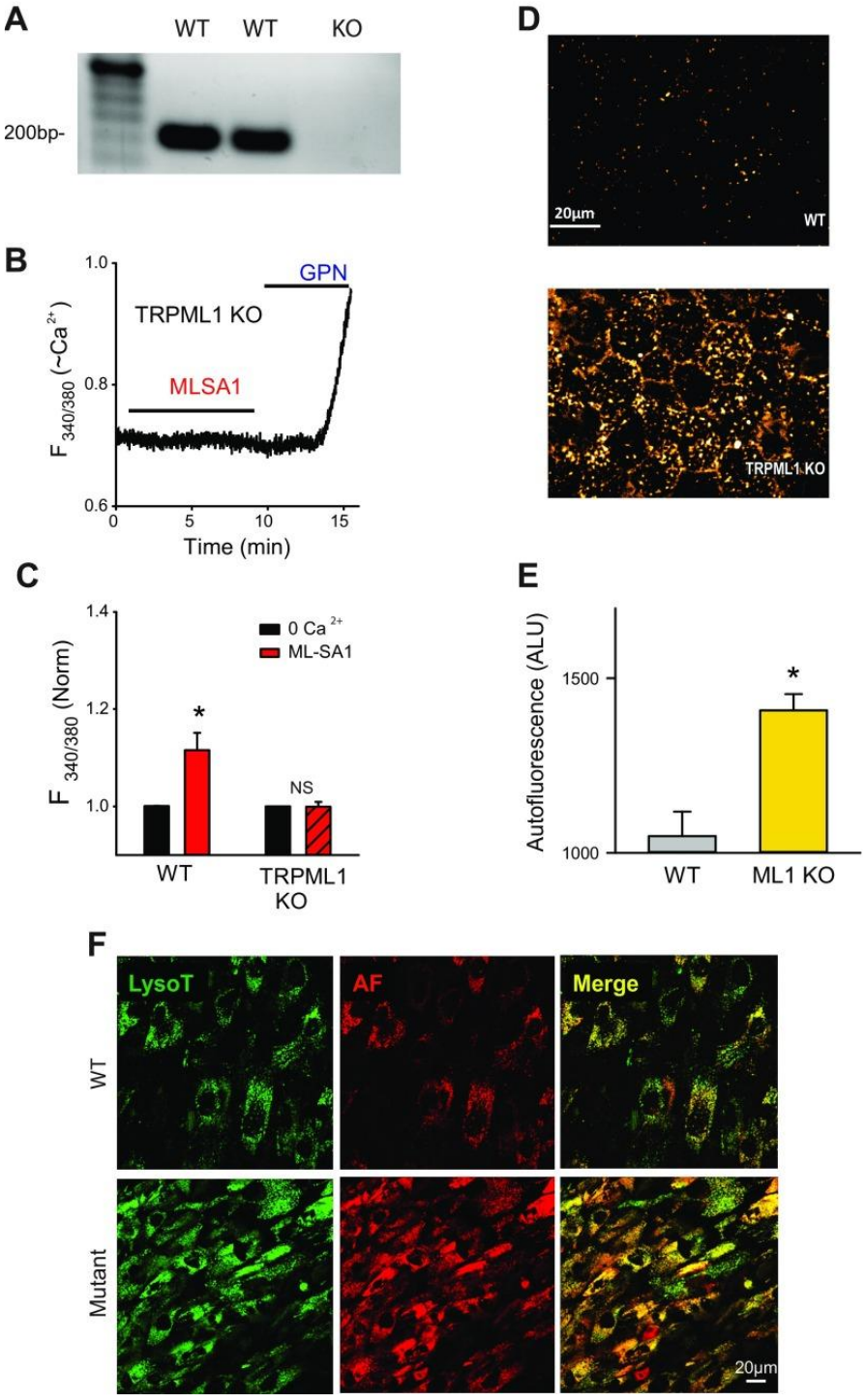

Role of TRPML1 channel. *A*) Genotyping of TRPML1$^{-/-}$ mice showing the presence of PCR product at expected 203 bp in WT mice but not homozygous knockout mice. *B*) ML-SA1 (20 µM) failed to induce an increase in cytoplasmic calcium in RPE cells from TRPML1$^{-/-}$ mice. The calcium increase induced by 200 µM GPN demonstrates that the lysosomes contained stores of calcium. *C*) Quantification of the increase in cytoplasmic calcium in RPE cells from WT ($P = 0.008$; $n = 5$) and TRPML1$^{-/-}$ mice ($n = 3$) NS, not significant. *D*) RPE whole mounts from 8-mo-old WT (top) and TRPML1$^{-/-}$ (bottom) mice showing increased autofluorescence in the knockout. The hexagonal shapes of the RPE cells are outlined by the autofluorescent granules. *E*) The levels of autofluorescence at 488 nm ex as arbitrary light units (ALU) in RPE cells from control and TRPML1$^{-/-}$ (ML1KO) mice. *$P < 0.001$ ($n = 30$). *F*) Greater levels of autofluorescence (red) and staining for LysoTracker (green) in fibroblasts from patients with MLIV (mutant) than control (WT).

Figure 5.

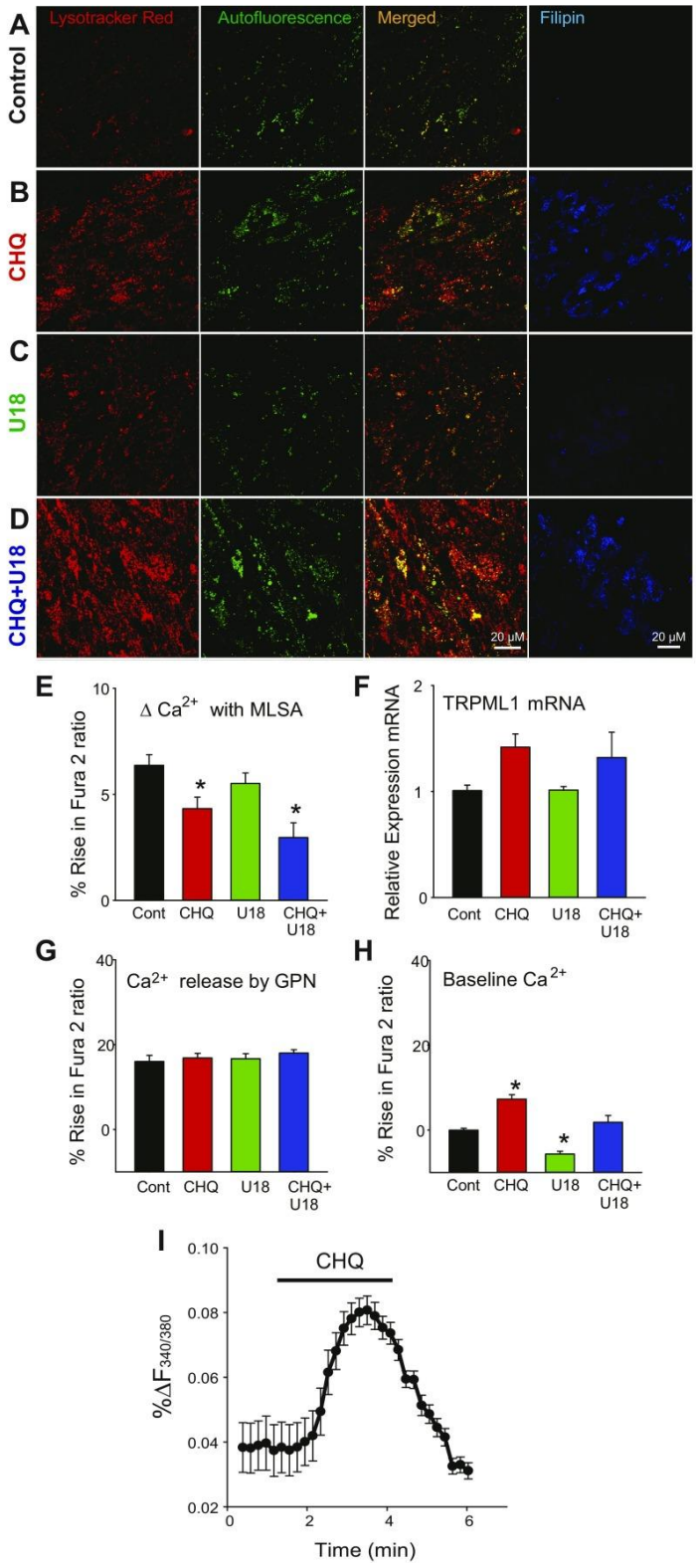

Lysosomal lipid accumulation impairs release of Ca^{2+} by ML-SA1. *A–D*) Representative images of ARPE-19 cells exposed to different conditions. *A*) Seven days under control conditions. *B*) Seven days of 10 μM CHQ. *C*) Six days under control conditions and 24 h 1 μM U18666A. *D*) Six days of 10 μM CHQ and 24 h 1 μM U18666A + 10 μM CHQ. Staining for LysoTracker Red (ex/em 563/590 nm) and autofluorescence (ex/em 488/525 nm) were obtained in the same cells by live imaging confocal microscopy; the overlap in yellow indicates that most autofluorescence was associated with lysosomes, but distinct areas of red and green indicate the signals were independent. Staining with filipin (ex/em 406/470 nm) indicates vesicular

cholesterol. *E*) Levels of cytosolic calcium in response to ML-SA1 were reduced in cells treated with CHQ and CHQ/U18666A. **P* < 0.001 *vs.* control (*n* = 24–32 wells from 4 plates). *F*) The reduced release of Ca^{2+} by ML-SA1 in cells treated with 10 μM CHQ and 10 μM CHQ + 1 μM U18666A did not reflect a difference in expression of *TRPML1* mRNA as determined using qPCR (*n* = 3). *G*) This did not reflect changes in the total levels of Ca^{2+} because lysing with GPN released the same levels of calcium. Not significant at *P* = 0.665 (*n* = 14–15 wells from 3 plates), normalized to ratios before GPN exposure. *H*) Levels of basal cytoplasmic calcium were increased in the presence of CHQ and decreased in the presence of U18666A, and no change was seen in the presence of CHQ + U18666A. **P* < 0.001 *vs.* control (*n* = 24–32 wells from 4 plates). *I*) Short-term exposure to CHQ (10 μM) elevates cytoplasmic calcium in ARPE-19 cells. Means ± SEM (*n* = 7). Presented as change in Fura-2 ratio from minimum.

Figure 6.

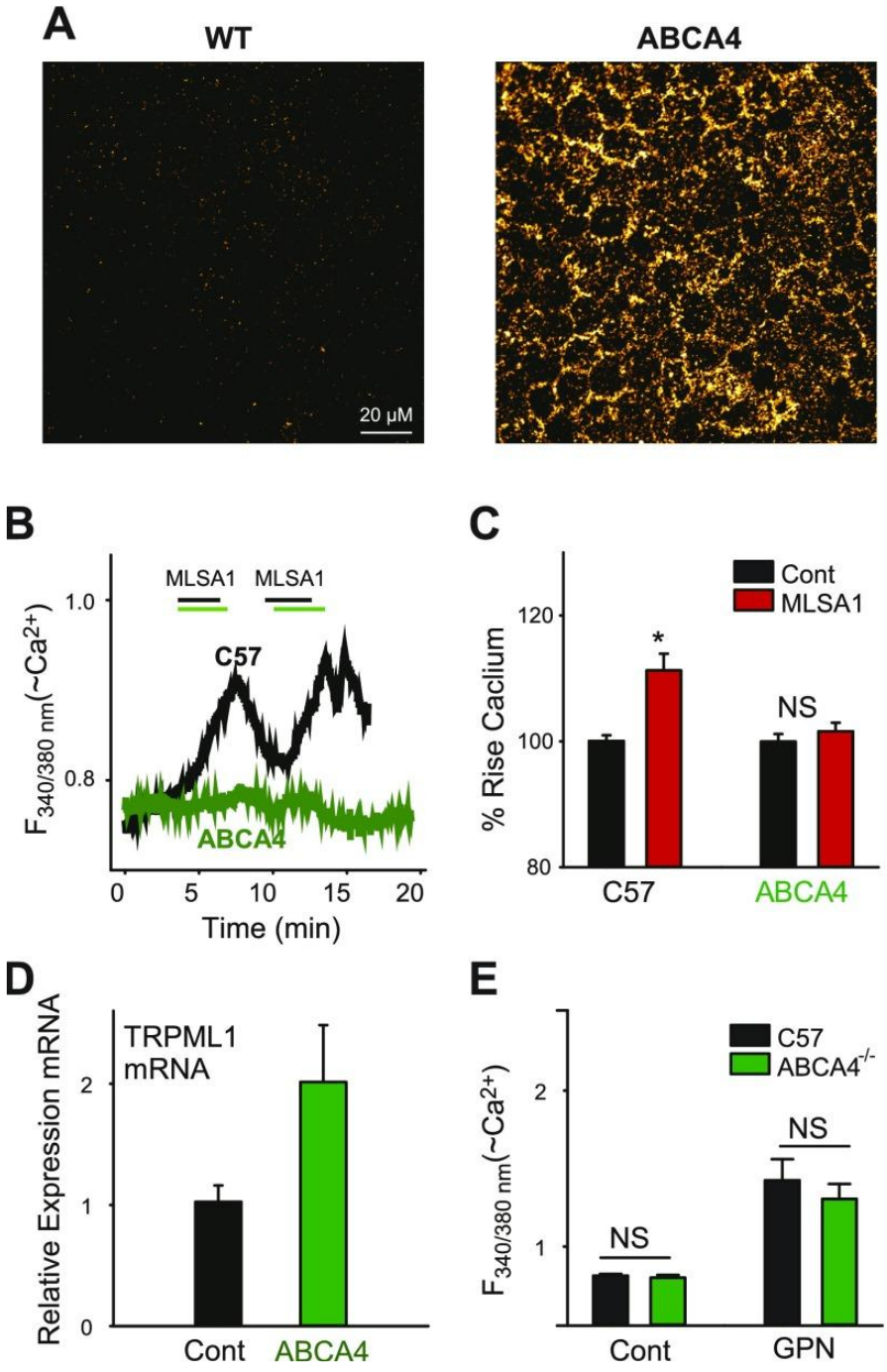

Defective calcium release in RPE cells from ABCA4$^{-/-}$ mice. *A*) Autofluorescence in RPE cells from control (left) and ABCA4$^{-/-}$ mice (right). Concentrated levels of lipofuscin were observed to congregate along the basolateral membranes of the cell. *B*) Representative trace showing the change in the $F_{340/380}$ Ca^{2+} signal in response to 20 μM ML-SA1 in RPE cells from ABCA4$^{-/-}$ mice compared with control. *C*) Quantitation of the mean response. Control, n = 21 cells; ABCA4$^{-/-}$, n = 17 cells. *P < 0.001 *vs.* untreated. *D*) Expression of *TRPML1* mRNA. P = 0.067 (n = 4). *E*) The lysosomal Ca^{2+} released by 200 μM GPN was not significantly different in RPE cells from ABCA4$^{-/-}$ mice.

Figure 7.

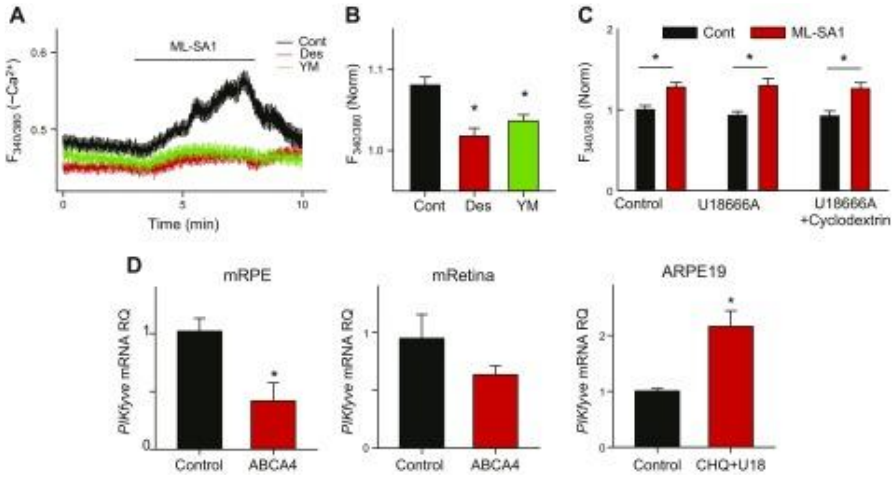

Pathways regulating Ca^{2+} release triggered by ML-SA1. *A*) Representative trace showing the change in the $F_{340/380}$ Ca^{2+} signal in response to 20 μM ML-SA1 in ARPE-19 cells treated with the acid sphingomyelinase inhibitor desipramine (Des, red, 10 μM; $n = 14$) or the PIKfyve inhibitor YM201636 (YM, green, 1 μM, $n = 13$) is reduced as compared with untreated control cells [control (cont), $n = 19$]. Cells in Ca^{2+}-free solution. *B*) Means ± SEM values for the increase triggered by 20 μM ML-SA1 in ARPE-19 cells treated with Des, YM, and control. *$P < 0.001$ *vs.* control ($n = 36$, 49, and 54 cells, respectively, from 4 coverslips each). *C*) Treatment with 300 μM cyclodextrin for 24 h to decrease cholesterol had no effect on the response to 20 μM ML-SA1 in cells treated with only U18666A ($n = 35–43$ cells from 4 separate coverslips each). *$P < 0.05$, ML-SA1 *vs.* control. *D*) Results from qPCR showing expression of enzyme PIKfyve in RPE cells (left) or retina (center) from 16-mo-old $ABCA4^{-/-}$ mice as compared with age-matched control mice. *$P = 0.023$ ($n = 3–4$). Expression of PIKfyve in ARPE-19 cells treatment with 10 μM CHQ for 7 d and U18666A for 1 d is increased (right). $P = 0.002$ ($n = 6$).